

The CUORE cryostat: an infrastructure for rare event searches at millikelvin temperatures

C. Alduino,¹ F. Alessandria,² M. Balata,³ D. Biare,⁴ M. Biassoni,⁵ C. Bucci,³ A. Caminata,⁶ L. Canonica,^{7,3,*} L. Cappelli,^{3,8,4} G. Ceruti,⁵ A. Chiarini,⁹ N. Chott,¹ M. Clemenza,^{10,5} S. Copello,^{11,3} A. Corsi,³ O. Cremonesi,⁵ A. D'Addabbo,³ S. Dell'Oro,¹² L. Di Paolo,³ M. L. Di Vacri,^{3,13} A. Drobizhev,^{8,4} M. Faverezani,^{10,5} E. Ferri,^{10,5} M. A. Franceschi,¹⁴ R. Gaigher,⁵ L. Gladstone,⁷ P. Gorla,³ M. Guetti,³ L. Ioannucci,³ Yu. G. Kolomensky,^{8,4} C. Ligi,¹⁴ L. Marini,^{8,4} T. Napolitano,¹⁴ S. Nisi,³ A. Nucciotti,^{10,5} I. Nutini,^{3,11} T. O'Donnell,¹² D. Orlandi,³ J. L. Ouellet,⁷ C. E. Pagliarone,^{3,15} L. Pattavina,³ A. Pelosi,¹⁶ M. Perego,⁵ E. Previtali,⁵ B. Romualdi,³ A. Rotilio,³ C. Rusconi,^{1,3} D. Santone,^{3,17} V. Singh,⁸ M. Sisti,^{10,5} L. Taffarello,¹⁸ E. Tatananni,³ F. Terranova,^{10,5} S. L. Wagaarachchi,^{8,4} J. Wallig,¹⁹ and C. Zarra³

¹*Department of Physics and Astronomy, University of South Carolina, Columbia, SC 29208, USA*

²*INFN – Sezione di Milano, Milano I-20133, Italy*

³*INFN – Laboratori Nazionali del Gran Sasso, Assergi (L'Aquila) I-67100, Italy*

⁴*Nuclear Science Division, Lawrence Berkeley National Laboratory, Berkeley, CA 94720, USA*

⁵*INFN – Sezione di Milano Bicocca, Milano I-20126, Italy*

⁶*INFN – Sezione di Genova, Genova I-16146, Italy*

⁷*Massachusetts Institute of Technology, Cambridge, MA 02139, USA*

⁸*Department of Physics, University of California, Berkeley, CA 94720, USA*

⁹*INFN – Sezione di Bologna, Bologna I-40127, Italy*

¹⁰*Dipartimento di Fisica, Università di Milano-Bicocca, Milano I-20126, Italy*

¹¹*INFN – Gran Sasso Science Institute, L'Aquila I-67100, Italy*

¹²*Center for Neutrino Physics, Virginia Polytechnic Institute and State University, Blacksburg, Virginia 24061, USA*

¹³*Dipartimento di Scienze Fisiche e Chimiche, Università dell'Aquila, L'Aquila I-67100, Italy*

¹⁴*INFN – Laboratori Nazionali di Frascati, Frascati (Roma) I-00044, Italy*

¹⁵*Dipartimento di Ingegneria Civile e Meccanica,*

Università degli Studi di Cassino e del Lazio Meridionale, Cassino I-03043, Italy

¹⁶*INFN – Sezione di Roma, Roma I-00185, Italy*

¹⁷*Dipartimento di Scienze Fisiche e Chimiche, Università dell'Aquila, L'Aquila I-67100, Italy*

¹⁸*INFN – Sezione di Padova, Padova I-35131, Italy*

¹⁹*Engineering Division, Lawrence Berkeley National Laboratory, Berkeley, CA 94720, USA*

(Dated: July 15, 2019)

The CUORE experiment is the world's largest bolometric experiment. The detector consists of an array of 988 TeO₂ crystals, for a total mass of 742 kg. CUORE is presently taking data at the Laboratori Nazionali del Gran Sasso, Italy, searching for the neutrinoless double beta decay of ¹³⁰Te. A large custom cryogen-free cryostat allows reaching and maintaining a base temperature of ~ 10 mK, required for the optimal operation of the detector. This apparatus has been designed in order to achieve a low noise environment, with minimal contribution to the radioactive background for the experiment. In this paper, we present an overview of the CUORE cryostat, together with a description of all its sub-systems, focusing on the solutions identified to satisfy the stringent requirements. We briefly illustrate the various phases of the cryostat commissioning and highlight the relevant steps and milestones achieved each time. Finally, we describe the successful cooldown of CUORE.

Published on: Cryogenics **102**, 9 (2019)

DOI: [10.1016/j.cryogenics.2019.06.011](https://doi.org/10.1016/j.cryogenics.2019.06.011)

I. INTRODUCTION

The Cryogenic Underground Observatory for Rare Events (CUORE) is a search for the Neutrinoless Double Beta Decay ($0\nu\beta\beta$ decay) of ¹³⁰Te [1, 2] at the Laboratori Nazionali del Gran Sasso (LNGS) in Italy. CUORE uses an array of 988 cryogenic bolometers [3] and is the largest bolometric experiment in the world. The total active

mass of the detector is 742 kg, with about 206 kg of ¹³⁰Te. In order to achieve the sensitivity goals of CUORE [4], the CUORE cryogenic system must meet a set of very tight design constraints on temperature, operational stability, noise environment, radioactive background and shielding. To achieve these, CUORE uses a custom-designed cryogen-free cryostat to host and cool the detector down to its operational temperature of ~ 10 mK.

The CUORE setup is hosted inside a building in Hall A of the LNGS underground laboratories, where the working volume of the cryostat protrudes into one of the CUORE cleanrooms. The high cleanliness standards reduced the risk of recontaminating the various parts dur-

* Present address: Max Planck Institut für Physik, D-80805, München, Germany

ing the commissioning phase and allowed for safe installation of the detectors.

A schematic of the CUORE cryostat is shown in Fig. 1. The cryostat consists of six nested vessels, the innermost of which contains the experimental volume. The different stages step the temperature down from room temperature to ~ 10 mK, and are identified by their approximate temperatures: 300 K, 40 K, 4 K, 800 mK or Still, 50 mK or Heat EXchanger (HEX), and 10 mK or Mixing Chamber (MC).

The 300 K and the 4 K vessels are vacuum-tight and define two vacuum volumes called the Outer Vacuum Chamber (OVC) and the Inner Vacuum Chamber (IVC), respectively. Two lead shields, inside the IVC, shield the detectors from external radioactivity. The Inner Lead Shield (ILS) stands between the 4 K and the Still stages and provides lateral shielding as well as shielding from below. The Top Lead is positioned below the MC plate and provides shielding from above. The CUORE detector is attached to the Tower Support Plate (TSP) placed right below the Top Lead.

Cooling is provided through three different systems. The Fast Cooling System (FCS) provides cooling from room temperature during the initial phase of a cooldown. A set of five Pulse Tube (PT) refrigerators cool the 40 K and 4 K plates. The lower stages, along with the detector, are further cooled by a custom-built $^3\text{He}/^4\text{He}$ Dilution Unit (DU).

The cryostat also embeds the Detector Calibration System (DCS), which allows deploying radioactive sources for calibrating the detectors (see Ref. [5] for details).

In the following sections, we overview the CUORE cryogenic infrastructure. In Sec. II, we discuss the mechanical design of the CUORE cryogenic system, the cryostat and detector support structures, the vibration isolation, and the materials selection. In Sec. III, we describe the cryogenic vacuum systems. In Sec. IV, we detail the cooling subsystems and the cooldown process. In Sec. V, we discuss the commissioning of the CUORE cryostat and in Sec. VI we describe the cooldown of the CUORE detector.

II. CRYOSTAT DESIGN

The design of the CUORE cryostat represented a significant challenge in the field of the refrigeration technology, coping with a challenging broad range of requirements:

- the experimental volume had to be sufficiently spacious to host the detector and part of the shielding (~ 1 m³);
- the detector base temperature had to allow the operation of the bolometers in optimal conditions. From the past experience, the working temperature was ~ 10 mK [6, 7];

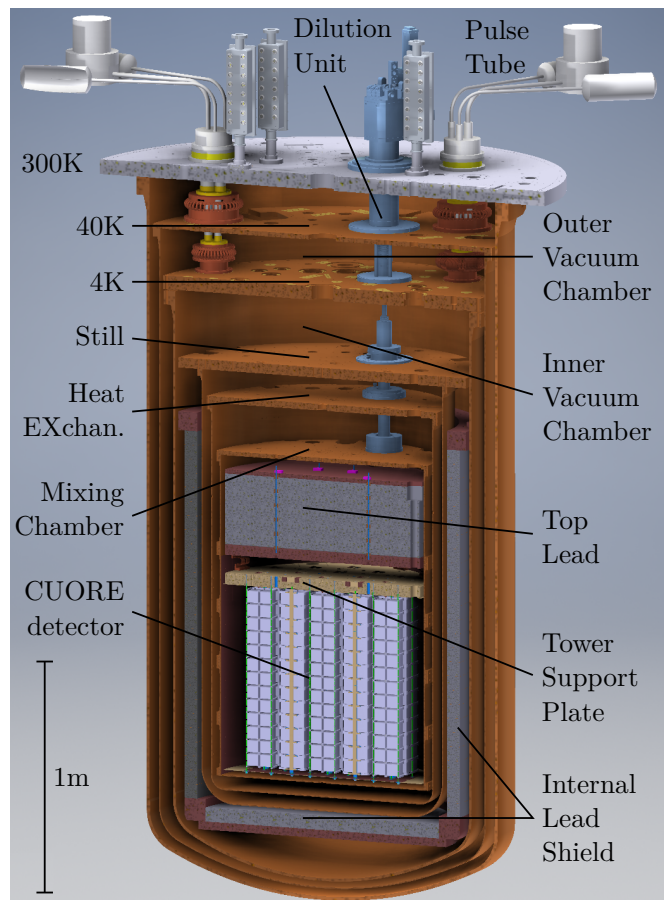


FIG. 1. Rendering of the CUORE cryostat. The different thermal stages, vacuum chambers, cooling elements and lead shields are indicated.

- the system had to be instrumented with ~ 2600 twisted pair NbTi wires for the detector readout and heater control [8, 9];
- the background coming from the natural radioactivity of the cryogenic materials had to be compatible with the CUORE sensitivity goal, which demands a total background rate ≤ 0.01 counts keV⁻¹ kg⁻¹ yr⁻¹ around 2.5 MeV [10];
- the system should be able to perform reliably over a several year run time with a very high duty cycle to maximize the live-time of the experiment;
- since LNGS is located in a seismically active area, the design had to take into account fail-safe mechanisms to limit damage in case of earthquakes.

The cryostat design began with a conservative thermal budget, supported by numerical modeling, subject to the available refrigeration technologies in 2007-2008, but required several iterations to make sure that enough cooling power was available for any unaccounted for thermal loads. One crucial early decision was the use of a

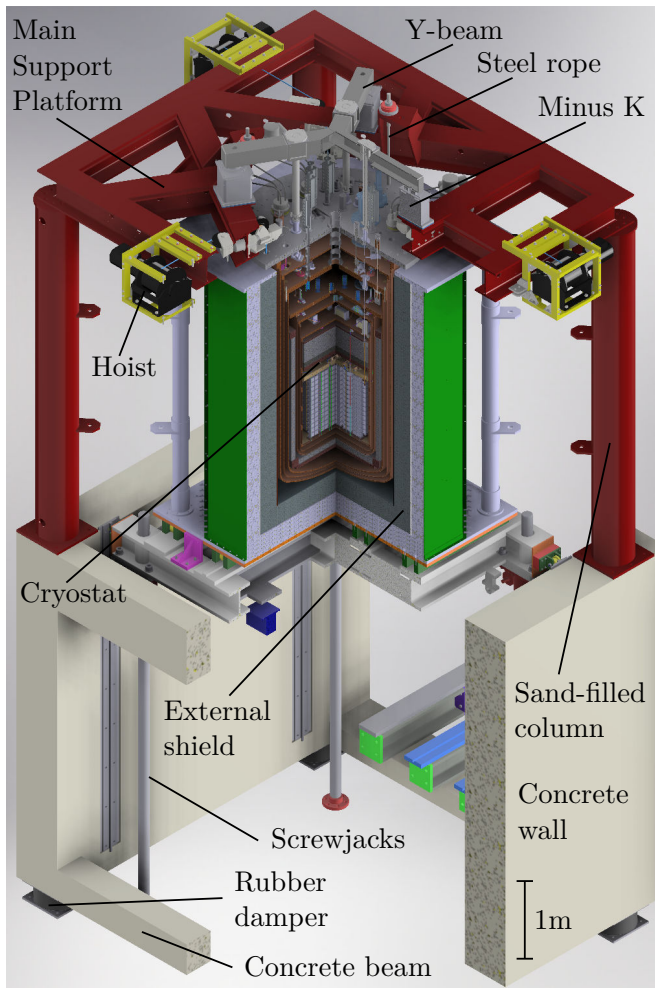


FIG. 2. Rendering of the cryostat support structure. The external lead shield sits on a movable platform and can be raised into place during the detector operation by four screwjacks. When the external lead is lowered, a false floor can close the cryostat and detector into a cleanroom environment.

“dry” system with multiple PTs, instead of a conventional “wet” system which uses a liquid helium bath. This increases the uptime fraction by eliminating the need for He refills, but introduces vibrational challenges. We also chose to use a powerful custom-built $^3\text{He}/^4\text{He}$ dilution refrigerator instead of an off-the-shelf dilution unit.

A. Mechanical support

The cryostat support structure (Fig. 2) has the double function of being a mechanical support for the cryostat while isolating the cryostat from the rest of the host building and surrounding environment. Further, it must satisfy the earthquake safety requirements for the region. As a result, its design is based on a deep seismic analysis, that has been performed to study the structural response

of the system to seismic events [11].

The lower structure forms the basement and consists of two 60 cm thick walls 4.5 m tall by 4.5 m wide connected at the corners by three concrete beams.¹ Each wall rests on two rubber dampers with high damping coefficients, which effectively decouple the structure from the ground. On top of the walls, four tubular 4.25 m tall sand-filled steel columns are installed at the corners. The Main Support Platform (MSP) sits on top of these columns and consists of a 4.7 m \times 4.1 m grid of steel I-beams.

The 300 K plate is suspended from the MSP and sits at the level of the cleanroom ceiling. This plate separates the cleanroom environment, below, from the non-cleanroom environment, above. The area above the 300 K plate and MSP holds both the plumbing to operate the cryostat as well as the detector front-end electronics inside a Faraday Room [12].

The MSP supports the full weight of the cryostat by means of three stainless steel ropes. Each rope is loaded with ~ 6 t and has been dimensioned to safely withstand the strongest expected earthquake with peak-ground-acceleration (PGA) = 0.26 g (the probability of occurrence is once in 475 years). All the cryostat components, though not the detector, are directly or indirectly held by the 300 K plate. Each cryostat plate is held by three vertical bars, that ensure a precise vertical alignment (Table I and Fig. 3). We performed dedicated measurements to characterize the conductivity of the bars at low temperature and verified that heat leakage through the supports were within the thermal budget [13].

The 300 K plate holds the 40 K, 4 K and Still plates. The support bars have been designed to be loaded each with about 0.33, 0.66 and 3.2 t respectively. These can resist without damage only more frequent and weaker earthquakes, namely those with PGA ~ 0.08 g (the probability of occurrence is once in 35 years). The 40 K, 4 K and Still plates are suspended from the OVC top plate by means of three independent sets of 316LN stainless steel bars. The bar support are constituted by tilting CuBe gimbals designed to prevent damage to the loaded rods in case of a shield displacement caused by a seismic event.² In particular, on the 4 K plate, the vacuum tight access of the Still bars entering the IVC is achieved by metallic bellows welded on the bars themselves. The HEX plate is held by the Still plate and supports the MC plate in turn. The support rods are attached to the plates using articulated joints and gimbals to allow relative movement between the individual stages. This prevents structural damage during seismic events.

¹ A fourth concrete beam was excluded because it would have prevented movement of the external shielding. A still brace (not shown in the figure) was installed at the end of the cryostat commissioning (see Sec. V) to comply with the safety regulations.

² At the end of the cryostat commissioning phase, the bottom gimbals of the Still support bars have been replaced by brass cylinders in order to reduce the transmission of vibrations, which would have spoiled the detector performance (Sec. V F)

TABLE I. Details of the cryostat support structure. For each plate and shield, the mechanical mount point, the distance to the above stage and the characteristics of the support bars (material and geometry) are shown. The Top Lead and TSP have multiple support stages, which are listed from top to bottom. See also Fig. 3.

Plate	Mount Point	Dist. [mm]	Material	Diam. [mm]	Joints
300 K	MSP	750	steel	22	steel joints
40 K	300 K	195	SS 316LN	8	CuBe gimbals
4 K	300 K	198	SS 316LN	7.5	CuBe gimbals
Still	300 K	287	SS 316LN	18	CuBe gimbals
HEX	Still	112	Ti6Al4V	6	steel joints
MC	HEX	202	Ti6Al4V	4	steel joints
ILS	Still	187	steel	20	steel threaded bushings
Top Lead	300 K [†]	60	SS 316LN	8.7	steel /
	Still		Kevlar K49	8 × 2	copper
	MC		Cu NOSV	12.2	blocks
TSP	Y-beam	76.8	SS 316LN	12	steel /
	300 K [†]		SS 316LN	6	copper
	Still		Kevlar K49	6 × 2	block
	MC		Cu NOSV	9.3	

[†]segmented: 300 K – 40 K / 40 K – 4 K / 4 K – 4 K / 4 K – Still

Each plate holds a corresponding vessel, which encloses the colder volume and acts as thermal radiation shield. Due to the large masses, the vessels are raised and lowered by a system of three synchronized hoists, which are anchored to the MSP.

The ILS is mechanically supported by the Still plate, but thermalized to the 4 K plate. The Top Lead hangs directly from the 300 K plate through a set of vertical bars that pass through each of the plates above, but is thermalized to the HEX plate.

The detector is mounted to the TSP and decoupled from the rest of the cryostat infrastructure.

B. Vibration isolation

Mechanical vibrations generate unwanted heat loads through microfrictions. These can dissipate power on

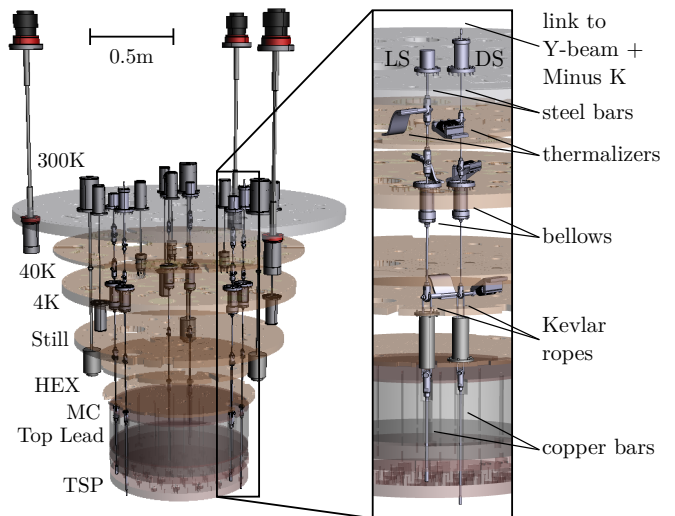


FIG. 3. Rendering of open cryostat with detailed view of the supporting elements. The zoom shows the details of the DS and LS components.

the coldest stages and can prevent stable operation at the desired temperature. The impact is even more severe on the bolometers themselves, which effectively act as heat-to-voltage amplifiers. Mechanical vibrations can impart stray power directly to the detector and this noise, along with microphonic noise, can spoil the energy resolution of the bolometers and directly impact the sensitivity of CUORE [14].

We adopted various solutions in order to minimize the effects of vibration on the colder stages and detector. The cryostat support structure is designed to mechanically isolate the colder stages from the warmer ones and from the surrounding environment. But this has to be balanced against the need to thermally couple the colder stages to efficiently remove heat and cool them. In particular, the PTs themselves are a significant source of vibration but must be thermally coupled. Hence, a significant effort is made to ensure that vibrational power is dissipated outside the cryostat.

1. PT decoupling

In general, PTs have no moving parts at their coldest stages, which significantly reduces the amount of noise generated during operation. However, the compressors and the rotating valves which drive the cooling are sources of mechanical vibrations. Further, the pressure waves generated by compressing and expanding the He gas cause a periodic deformation of all the gas lines and induce the cyclical expansion of the actual pulse tube, both along and perpendicularly to the PT axis. Without appropriate countermeasures, we found that the generated vibrational noise would be too high for detector operation.

To minimize the effects of vibrational noise, we start by

separating the PT compressors from the rest of the cryogenic infrastructure. The compressors are located ~ 15 m away from the 300 K plate and are supported by a metallic structure connected to the concrete ground below the CUORE hut via six elastomers. The incoming/outgoing He flexlines pass through a sandbox rigidly connected to the ground and filled with ~ 1.5 t of non-hygroscopic quartz powder. The sandbox absorbs a significant fraction of the vibration generated by the compressors. The high pressure lines are covered with neoprene to reduce the emission of acoustic noise. As the lines enter the Faraday Room, a set of ceramic decouplers electrically isolate the lines inside the room from outside and prevent the lines from transmitting electromagnetic noise into the room.

We separate the rotating valves from the PT heads (Fig. 8) and mount them separately from the MSP and 300 K plate. This solution removes all moving parts from the cryostat and thus reduces mechanical vibrations. Moreover, by electrically decoupling the valves from the PT (and cryostat) we electrically isolate the PT compressors from the detector grounds. Each PT head is connected to the 300 K plate via a polyurethane ring which absorbs part of the incoming vibrations, while a sliding seal compensates for the vertical displacement of the PT due to the thermal contractions at the cold stages (Fig. 1). Despite decoupling from the 300 K plate, vibration is still transferred down the PT itself and could be deposited on the lower plates. Therefore, the PT cold stages are thermally linked to the 40 K and 4 K plates through a set of flexible thermal links (copper braids), making a softer connection and reducing vibration transfer to the plates themselves.

Separating the rotating valves from the PT head also mitigates the effects of the He pressure waves, by allowing all contraction and expansion to be absorbed by movement of the valve itself. The rotating valves and gas expansion vessels are attached to the compressors through a set of custom high pressure lines which run along the ceiling of the Faraday room. The pressure lines and rotating valves are supported by a set of bungee cords anchored to the ceiling of the Faraday Room, allowing constrained movement of the valves and lines. This design dissipates vibrations into the cords and the Faraday Room, and away from the MSP and 300 K plates.

Finally, instead of using the standard stepping motor embedded in the PT compressors, the CUORE rotating valves are driven by microstepping motors specifically intended for situations where motor vibrations must be minimized. These custom drivers also allow for control over the relative phases of the running PT pressure oscillations and tune them to a configuration that minimizes vibration transmission to the detector [15].

2. Detector decoupling

In order to further reduce vibration transfer from the cooling infrastructure, the CUORE detector is mechanically decoupled from the cryostat. The detector, mounted to the TSP, hangs from a steel Y-beam positioned on top of three MinusK vibration isolators [16] directly anchored to the MSP (Fig. 2). Each isolator behaves like a soft spring when subjected to small displacements, despite the heavy load it bears (~ 1 tonne in total). This behavior favors very low natural frequencies for the spring-mass system, with a cut-off frequency of close to 0.5 Hz (see Ref. [17] for details).

The connection between the TSP and the Y-beam is made by means of the Detector Suspension (DS) system. The DS system, as well as the Lead Suspension (LS) system that supports the Top Lead, consists of three segmented vertical bars (Fig. 3 and Table I). The top part, from the Y-beam (or 300 K plate for the LS) down to the Still level, is made of segmented steel rods, which are thermalized at each cold stage and pass into the OVC and IVC through a set of vacuum-tight bellows. From the Still down to through the MC each support consist of a pair of Kevlar ropes, which minimize heat transfer down to the coldest stages.³ Finally, the TSP is supported from the bottom of the Kevlar ropes through a set of high purity copper rods, chosen for their low radioactivity content.

C. Materials

One of the main goals of the CUORE cryostat is to create a low background environment for the CUORE detector to search for $0\nu\beta\beta$ decay and other rare events. This places strong constraints on the materials chosen to build the various components of the cryogenic infrastructure, as well as on their handling and storage. A major challenge was to select materials which had minimal bulk Th and U contamination, while still being compatible with the low temperature thermal requirements. We carried out an extensive campaign of radio-assaying to select materials and production techniques for all components. The resulting activity measurements and upper limits are used as input to a detailed Monte Carlo simulation to evaluate the expected background for CUORE [10].

The majority of the structural cryostat components, including the plates and vessels, are made from copper (Table II). A significant exception is the 300 K plate and the upper part of the 300 K vessel flange, which are made from austenitic stainless steel. The use of stainless steel provides a more reliable vacuum seal and more mechanical strength against the huge load across the area of the

³ The cryogenic properties of Kevlar K49 have been studied in a dedicated measurement, focusing on the long-term mechanical creeping [18].

TABLE II. Cryostat mass inventory.

Part	Diam. [mm]	Height [mm]	Thick. [mm]	Material	Mass [kg]
<i>Vessels</i>					
300 K plate	2060	62	-	SS 304L	1540
300 K shield	1603	2620	12/15	Cu OFE	1600
		410	12	+ SS 304L	370
40 K plate	1573	20	-	Cu OFE	300
40 K shield	1503	2765	5	Cu OFE	680
4 K plate	1473	59	-	Cu OFE	830
4 K shield	1363	2471	10/12	Cu OFE	1160
Still plate	1333	43	-	Cu OFE	500
Still shield	1110	1850	5	Cu OFE	340
HEX plate	1070	28	-	Cu OFE	220
HEX shield	1020	1650	5	Cu OFE	290
MC plate	980	18	-	Cu NOSV	110
MC shield	940	1365	5	Cu NOSV	340
<i>Lead shields</i>					
ILS (side)	1157	1568	60	Pb (Roman)	3920
ILS (bottom)	1080	60	-	Pb (Roman)	620
Ring (top)	1157	80	88	Cu OFE	240
Ring (bottom)	1080	95	98.5	Cu OFE	300
Plate (bottom)	1150	35	-	Cu OFE	320
Top Lead	900	300	-	Pb	2110
Plate (top)	900	18	-	Cu NOSV	90
Plate (bottom)	900	46	-	Cu NOSV	260
<i>Detector</i>					
TSP	900	48	-	Cu NOSV	260
Frames	-	-	-	Cu NOSV	67
Crystals	-	-	-	TeO ₂	742

plate. The lower plates and vessels down to the HEX, as well as the lower part of the 300 K vessel are made from oxygen-free electrolytic (OFE) C10100 copper, which has a purity of 99.99%. Assays of the CUORE OFE copper have placed upper limits on the ^{232}Th and ^{238}U activity at $< 6.5 \cdot 10^{-5} \text{Bq kg}^{-1}$ and $< 5.4 \cdot 10^{-5} \text{Bq kg}^{-1}$, respectively.⁴

The MC vessel, MC plate, and the TSP are made of electrolytic tough pitch copper, referred to here as NOSV copper [20]. This is the same copper used to produce

the frames for the CUORE detector. This type of copper was selected for its high thermal conductivity at low temperatures (Residual-resistance ratio $RRR \geq 400$), its low radioactivity, and for its low hydrogen content. The latter property is important since, at low temperatures, the slow conversion of ortho-hydrogen to para-hydrogen can create heat leaks, dissipating power on the coldest stages [21, 22]. A dedicated measurement of the heat leak by NOSV copper set an upper limit of 3.7pW g^{-1} , well below usual the value for standard copper [23]. Additionally, as the NOSV copper is some of the closest material to the CUORE detector, the limit on its radioactivity is even more stringent than on the OFE copper. After procurement, all copper has been stored underground at LNGS to minimize activation by cosmic radiation.

The lead shielding, inserted to protect the detector from the external radiation, underwent the material selection process as well. The ILS [24] is a 6 cm-thick lead vessel which shields the detector from the sides and bottom. The choice of lead for the ILS was critical, as this shield is only separated from the CUORE detector by ~ 1 cm of copper (i. e. the thickness of the HEX and MC vessel). In particular, the presence of ^{210}Pb creates a low energy background continuum in CUORE through the production of bremsstrahlung produced in its β -decay and that of the daughter ^{210}Bi . Because of this, the ILS is made of radio-pure lead of archaeological origin, with an upper limit on its ^{210}Pb bulk contamination of 4mBq kg^{-1} [25]. The Top Lead consists of five 6 cm-thick disks of commercial pure lead stacked and sandwiched between two copper plates. Here, the choice of lead was less critical since the Top Lead is separated from the detectors by over 9 cm of copper (i. e. the bottom plate of the Top Lead + the TSP). The ILS supports are made from high purity OFE copper, and the copper plates sandwiching the Top Lead are made from NOSV copper.

In order to reduce the amount of heat transferred from the warmer stages to the colder stages as radiation, we cover the vessels and plates of the 40 K and 4 K stages in Coolcat 2 NW thermal insulation by Ruag (referred to here as superinsulation). Each layer of superinsulation is composed of 10 double-sided aluminized, perforated polyester foil interleaved with 10 foils of non-woven polyester spacer material. The 40 K stage is wrapped with three such layers, while the 4 K stage is wrapped in one layer. Given the large surface area, this actually represents a significant mass of superinsulation of ~ 17 kg. However, despite its large mass, the superinsulation contributes negligibly to the radioactive background of the detectors [10].

III. VACUUM SYSTEMS

The CUORE cryostat has two separate vacuum chambers: the OVC, which comprises the 300 K vessel and the IVC, which comprises the 4 K vessel. The two nested vacuum chambers are essential for the cooldown process,

⁴ A detailed description of the vessel production and machining can be found in Ref. [19], where special attention is paid to the description of the welding techniques employed to minimize radioactive contamination during welding.

TABLE III. Maximum design differential pressures (inside vs. outside and outside vs. inside) for the OVC and IVC vessels that can be stood by the volumes during the different phases of operations.

Vessel	V [m ³]	ΔP_{\max} [bar]	
		$\Delta P_{\text{in-out}}$	$\Delta P_{\text{out-in}}$
OVC	5.86	0.1	1.01
IVC	3.44	1.5	1.1

which uses He exchange gas in the IVC to thermalize the colder cryostat stages.

The 300 K and the 4 K vessels must be able to withstand both internal and external overpressure without worsening the vacuum and avoiding plastic deformations. While the OVC is subject to ambient pressure, the IVC has to withstand ~ 1.3 bar of internal overpressure during the initial phase of the cooldown, when the FCS is operational (see Sec. IV A).

The wall thickness for the vacuum vessels were calculated according to the American Society of Mechanical Engineers (ASME) code [26] and we performed a linear buckling analysis with ANSYS [27] in order to ensure that we could reach the pressure requirements (Table III). The limiting differential pressures for the OVC and IVC vessels have been calculated to be 2.0 bar and 2.3 bar, respectively. A drop-off plate on the OVC and a rupture disk on the IVC prevent the internal pressure of each vessel from exceeding the environment pressure by 0.5 bar.

The pumping system consists of one turbomolecular pump for each volume backed by a single dry scroll pump. In particular, the IVC turbomolecular pump was selected for its elevated compression factor for He ($> 10^8$), which minimizes the presence of residual gas after the completion of the FCS phase of the cooldown. A charcoal getter (with integrated heater) placed below the 4 K plate inside the IVC helps in absorbing any He leftover.⁵

The seal between the 300 K plate and vessel is made with a Buna-N elastomer ring, selected for the low He permeability. For the IVC, the seal must hold at cryogenic temperatures and thus the connection between the 4 K plate and vessel is made by a Helicoflex™ seal [28] mounted inside a centering ring. In fact, elastomer o-rings cannot be used at cryogenic temperatures since they would freeze, while the use of both indium and Kapton sealings would be impractical given the dimension of the flange.

Elastomer o-rings are used to seal the various OVC and IVC ports at room temperature, while indium gaskets are used for the IVC ports on the 4 K plate.

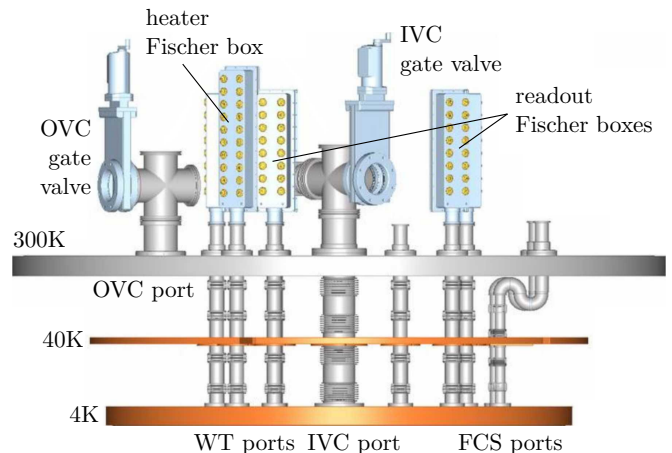


FIG. 4. Schematic of the OVC and IVC ports. The WT, heater and diagnostic sensor ports are connected to Fischer boxes. The OVC and IVC ports are closed gate valves for the pumping and the injection of gas. The FCS ports are sealed with blank flanges when the system is not in operation. The lines inside the cryostat are provided with bellows, which allows for the system flexibility in case of seismic events.

The OVC has 2 access ports (Fig. 4): 1 DN100 pumping port, and 1 DN40 wiring port for the readout of temperature and pressure sensors. The IVC has multiple access ports: 1 DN100 pumping port, 5 DN40 Wire Tray (WT) ports for the detector readout, 1 DN40 WT port for heater control, 1 DN40 WT port for readout of temperature and pressure sensors, and 2 DN40 ports for the inlet/outlet of the FCS He. Furthermore, there are 4 DN50 ports for the deployment of the radioactive sources with the DCS and 3 DN16 ports for the readout of the DU sensors embedded in the DU.

All the IVC ports are equipped with radiation baffles that prevent direct line of sight between the 300 K and the 4 K plates. The specific design of the radiation baffles depends on the dimension and occupancy of the port. For example, the IVC and FCS ports, which must allow for a large gas flow, have a series of double segmented baffles, while the WT ports have polytetrafluoroethylene (PTFE) spirals that guide the wires while simultaneously blocking direct radiation from the warmer stages.

IV. COOLDOWN SYSTEMS

The CUORE cryostat is cryogen-free and cooled by multiple PTs and a custom-built ³He/⁴He dilution refrigerator, since “standard” solutions were not available for its size and mass.

The PTs provide enough cooling power to back the DU and maintain the desired base temperature, but on their own would take too much time to bring the system down to 4 K to begin operation of the DU. The total cooled mass is 13.7 t, of which 12.7 t is cooled to 4 K or below (Tab. II). Between 300 K and 40 K, the cooling system

⁵ The charcoal getter was inserted at the end of the cryostat commissioning since its presence makes it difficult to perform leak tests.

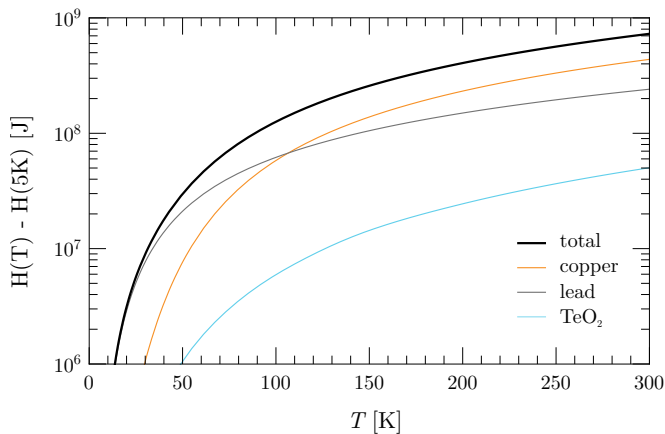


FIG. 5. IVC enthalpy as a function of the temperature. The contributions from the different materials are derived from the specific heat at different temperatures of copper [29], lead [30] and TeO_2 [31] and combined with the masses of each component (Table II).

must remove $\sim 6.9 \times 10^8$ J of enthalpy, which is over 95% of the total enthalpy of the system, (Fig. 5.) The cooling power of each of the five PTs is $\gtrsim 100$ W at 300 K, but decreases quickly at lower temperatures; by 100 K, the cooling power is already 50 W. The PTs alone, would imply a cooldown time of order of a few months.

Therefore, we designed a dedicated system to speed up the cooldown from room temperature, called the FCS [32, 33]. The system circulates He gas through a dedicated cooling circuit and injects the cold gas directly into the IVC. The FCS supports the PTs during the initial stages of the cooldown, until all stages inside the IVC reach $\lesssim 100$ K. The PTs then continue the cooldown until the DU can be activated and bring the system to base temperature.

Examples of the full cooldown are shown later in Secs. V E and VI.

A. Fast cooling system

The FCS consists of a separate cryostat cooled by three Gifford-McMahon (GM) cryorefrigerators AL600 made by Cryomech [34] (Fig. 6), and a compressor that forces the circulation of cold He gas through a dedicated circuit and into the IVC. The GM cooling power is much higher than that of a PT, being 1800 W at 300 K and 350 W at 50 K and a single unit embedded in the CUORE cryostat would have sufficed for the job. However, due to the lack of space and, especially, to the fact the GM would have created a significant thermal link between the 300 K and the 4 K stages during the normal operation, this solution was not practical. Hence the need for an external cryostat and multiple units.

A schematic of the circuit is shown in Fig. 7. The gas is cooled inside the FCS cryostat inside two heat exchangers: a counter-flow heat exchanger (HEX 1), and a series

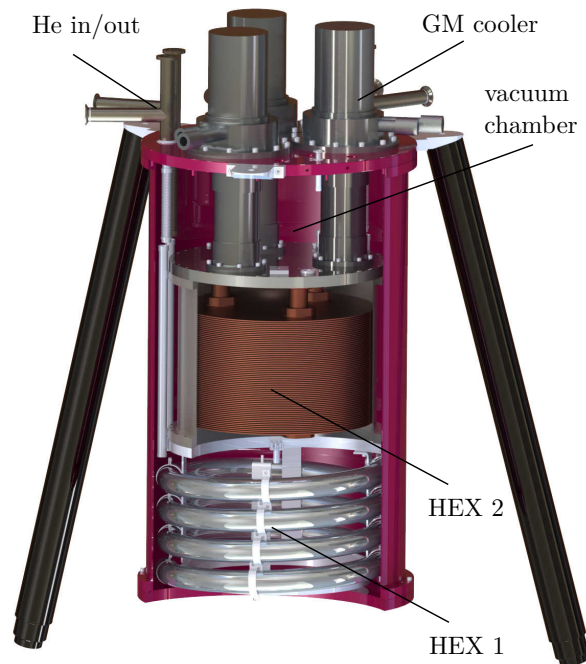


FIG. 6. Rendering of the FCS cryostat.

of Cu OFE plates directly connected to the cold stage of the GMs (HEX 2). In addition, a set of counter flow heat exchangers (HEX 0) precool the He as it enters the FCS cryostat.

As the cold gas enters the CUORE cryostat, it passes through an S-tube, which acts as a baffle to thermal radiation, and enters the IVC. From the 4 K plate, the cold He follows two paths. One guides the gas to the bottom of the ILS, while the other guides the He into the HEX and MC vessels through a set of PTFE tubes (chosen for low thermal conductivity and high radiopurity). The gas exits through a second port in the IVC plate and returns to the FCS cryostat.

We placed important constraints on the FCS:

- the IVC pressure must never exceed 1.3 bar to avoid any risk of damaging the cryostat vacuum seals;
- the circuit pressure must never be lower than the environmental pressure to prevent air from leak into the external pumping lines;
- the temperature inside the FCS cryostat should always be lower than 202 K (the Radon melting point) while circulating – this creates a cryo-pump for Rn and therefore prevents it from flowing into the CUORE cryostat;
- excessive temperature gradients must be avoided across the detector, due to its intrinsic fragility, and across the IVC vessel, to prevent deformations of the vacuum vessel.

These constraints require significantly limiting the pumping speed of the compressor, and hence reducing the sys-

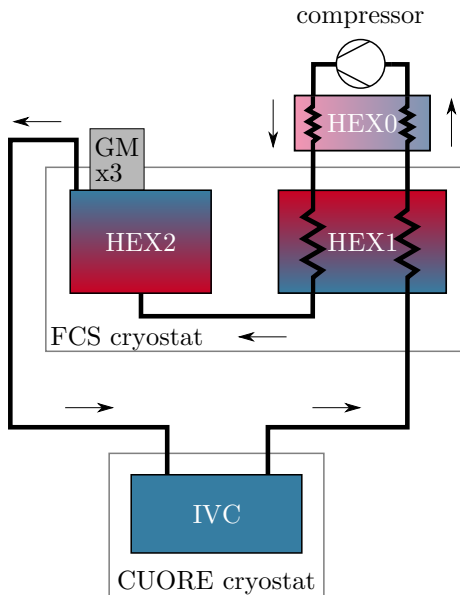


FIG. 7. Schematic of the FCS gas circuit. The arrows indicate the direction of the He flow.

tem cooling power. However, they ensure a safe cooldown for both the CUORE cryostat and detector. Even in these conditions, the FCS ensures a cooldown time within ~ 20 days (Figs. 14, 16 and 18).

At the beginning of the cooldown, a compressor frequency of ~ 20 Hz provides a larger gas flow. As the temperature decreases, the compressor frequency has to be constantly reduced down to a few Hz (Fig. 15). In the end, the minimum compressor frequency is limited by the parasitic power dissipation along the circuit, especially at the entrance/exit in the CUORE cryostat. Too low of a flow would result in a warm up of the circulating gas. Over the course of the cooldown, the temperature of the incoming He goes from ~ 150 K down to ~ 50 K. In order to maintain a constant pressure while the temperature decreases, we inject additional (clean) He gas.

The PTs are turned on a few days after the FCS, typically when the IVC temperatures are close to 200 K. By ~ 50 K, the PTs dominate the total cooling power and the FCS is turned off. The He is pumped out of the IVC, but we leave a few mBar of He to act as an exchange gas between the 4 K stage and the inner stages until they approach ~ 10 K.

B. Pulse tubes

The CUORE cryostat is cooled by five Cryomech PT415-RM pulse tube refrigerators [35] (Fig. 8). The choice of a dry system relying on PTs, over the conventional “wet” design which relies on liquid helium (LHe), was based on the both economic and logistic considerations. The wet system would require periodic LHe refills, which implies both a large cost, but also significant

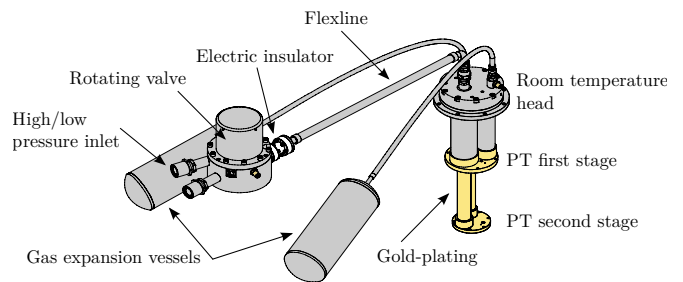


FIG. 8. Schematic of a CUORE PT (PT415-RM by Cryomech).

safety concerns given the amount of cryogen that would be needed. Instead, the dry system guarantees continuous operation, thus increasing the total duty cycle of the experiment.

The nominal cooling power of each PT is 32 W at 45 K (first stage) and 1.2 W at 4.2 K (second stage), while the lowest temperature achievable is close to 3 K in case of no thermal load. The choice of the remote motor-head option and 2 ft length of flexline between the PT and motor-head, fundamental to reduce the transmission of vibrations (see Sec. II B 1), implies a loss of $\sim 20\%$ in cooling power for the CUORE PTs.

Given this cooling power, a minimum of three PTs are required for normal operation. However, we decided to plan for the possibility that one PT could fail over the course of the experiment. This means accounting not only for the loss in cooling power, but also the additional heat load that an inactive PT implies.⁶ This required adding, not one, but two extra PTs. During normal operation, one of the five PTs is inactive.

To maximize the conductance between the cooling elements and the cryostat, the PT cold stages and the relevant sections of the cryostat plates are gold-plated. The copper braids, which constitute the actual thermal link, have high thermal conductivity at low temperatures ($RRR \geq 100$) and are gold-plated as well.

We can individually adjust the He pressure driving each PT, and optimize the cooling power of the system as a function of these pressures. Assuming working temperatures of 35 K and 3.5 K for the two thermal stages (see Sec. V), the cooling power of the 4 active PTs is ~ 80 W and ~ 2 W, respectively.

C. Dilution unit

The CUORE DU is a high-power custom CF-3000, manufactured by Leiden Cryogenics [36]. A schematic is shown in Fig. 9. The DU is a standalone element that

⁶ The power dissipation for an inactive PT415 was computed by Cryomech to be ~ 8.6 W at the first stage (between 300 K and 40 K) and ~ 0.4 W at the second stage (between 40 K and 4 K).

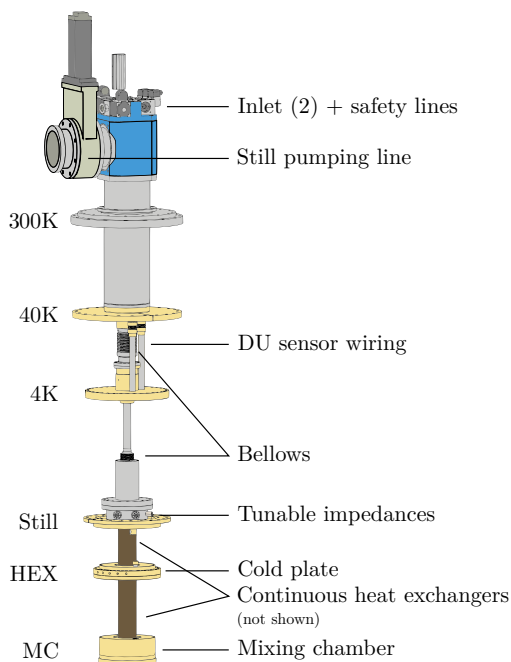


FIG. 9. Schematic of the CUORE DU (custom CF-3000 by Leiden Cryogenics).

can be inserted into the CUORE cryostat or into a separate dedicated test cryostat. In both cases, each thermal stage of the DU anchors to the corresponding plate. Similar to the PTs, the thermal connections are gold-plated to maximize the conductivity (the Still, HEX and MC plates are entirely gold-plated).

The CUORE DU has two parallel condensing lines through which the $^3\text{He}/^4\text{He}$ mixture is injected. Each line is thermalized between the stages of a PT, and then passes through a thermalizer anchored to the 4 K plate. The thermalizer ensures that the incoming mixture is still cooled down to 4 K even in the event that the PT that thermalizes the line fails. Below the 4 K plate, the mixture passes through an impedance that cools it to < 1 K through Joule-Thomson expansion. The impedance can be tuned while the cryostat is open. Apart from acting as a spare line for the mixture circulation during normal operation, the parallel condensing lines can be used simultaneously during the cooldown to increase the mixture flow rate and achieve a higher cooling power. The maximum flow rate using both lines is $\gtrsim 8 \text{ mmol s}^{-1}$.

The cooling power requirements on the DU were set by the goal of operating stably at a temperature of ~ 10 mK. In a conservative approach, the target base temperature for the “bare” DU was set to 6 mK. We extrapolated from simulations the cooling powers after the DU integration inside the CUORE cryostat, starting from the estimate of the thermal loads on the different stages. The main contributions at the coldest stages comprise the detector wiring, the DCS (guide tubes + irradiation from the sources during calibration), the detector and lead suspensions, and the cryostat support bars. We also added

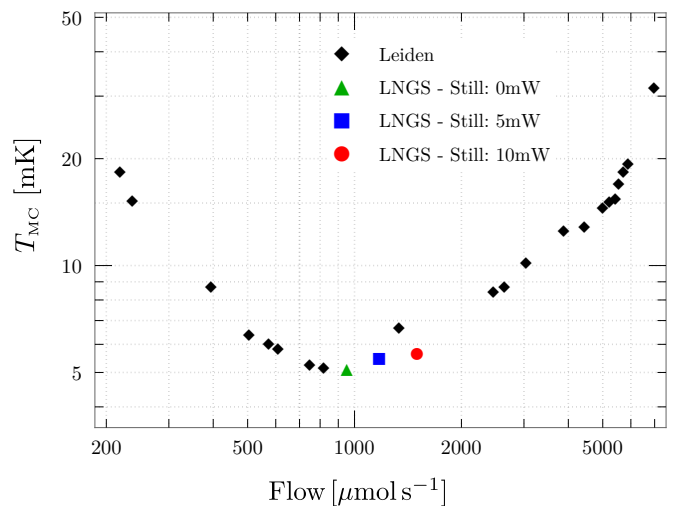


FIG. 10. Dependence of the MC temperature on the mixture flow. The black markers refer to the test performed at Leiden (August 2011). The colored markers refer to the test performed at LNGS inside a test cryostat (April 2013) and are the same shown in the bottom panel of Fig. 11 when no power is injected on the MC.

safety margins while computing the thermal loads, accounting for possible unknown sources besides the known ones.

The DU was characterized in the test cryostat, both at the construction site (Leiden, The Netherlands) and at LNGS. The dependence of the base temperature on the mixture flow was determined by injecting different powers on the Still and measuring the MC temperature and flow rate. The result is shown in Fig. 10 (black markers). The optimal value was found to be $\sim (800 - 1000) \mu\text{mol s}^{-1}$.

The cooling power of the DU was measured by injecting power directly on the MC stage (at fixed Still power) and observing the resulting base temperature. The results of the Leiden characterization are shown in the top panel of Fig. 11. The obtained values were 2 mW at 100 mK, 3 mW at 123 mK and 4 μW at 10 mK – these results actually exceeded the required specifications. The LNGS characterization focused on the DU behavior close to the base temperature, and the results are shown in Fig. 10. The LNGS results were compatible with the Leiden results when no power was injected on the Still, while the DU performance improved to $\sim 6 \mu\text{W}$ at 10 mK with a mixture flow of $1500 \mu\text{mol s}^{-1}$.

V. COMMISSIONING

The cryostat commissioning proceeded in phases, with a series of runs characterized by specific sub-goals (Table IV). As new components were integrated into the cryostat (Table V), they were tested in a cooldown.

In order to monitor the status during the cooldown

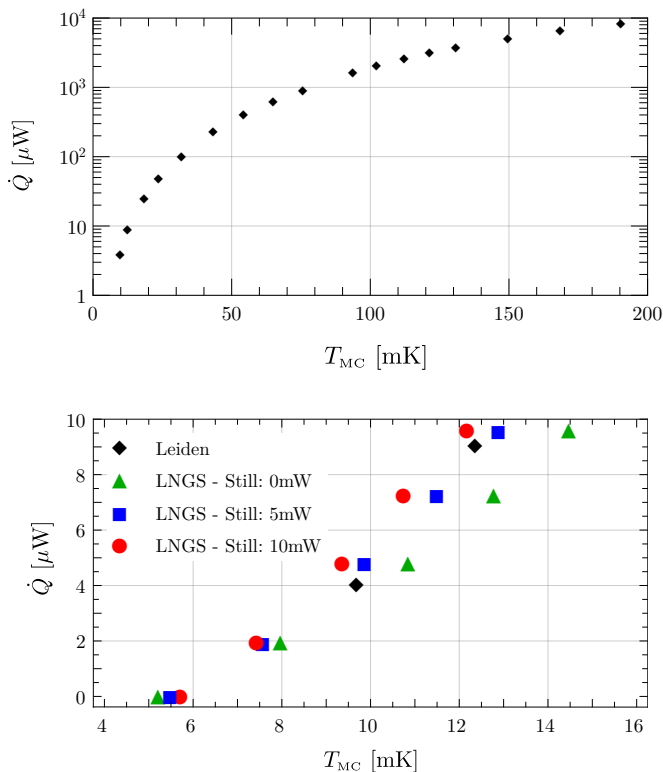


FIG. 11. DU cooling power as a function of the MC temperature. (Top) Test performed at Leiden. (Bottom) Zoom of the lowest temperature region with the inclusion of LNGS test results. The latter results show a better performance of the DU for increased power on the still.

and stable operation, more than 50 thermometers have been installed in the CUORE cryostat for diagnostic purposes. The temperatures of the various components of the cryostat are monitored by multiple thermometers for redundancy. Given the broad range of values, from environmental temperature (~ 295 K) down to detector base temperature (< 10 mK), we use different sets of thermometers. Temperatures down to a few kelvin are recorded by commercial silicon diode resistance thermometers. For temperatures below 1 K to a few tens of milikelvin, we use both commercial and custom made ruthenium oxide resistor thermometers. Finally, on the MC plate, we use an MFFT-1 Noise Thermometer by Magnicon [37] as well as a Cerium Magnesium Nitrate thermometer to monitor temperatures all the way down to a few milikelvin. These sensors are calibrated to a Superconducting Fixed Point device also installed on the MC plate. Below the Top Lead, bulk radioactivity places constraints on the sensor choice. Therefore, above a few kelvin, the detector temperature is monitored by “bare chip” diode thermometers. Once at base temperature, we use neutron transmutation doped (NTD) Ge thermistors for both temperature monitoring and for temperature stabilization.

In the end, the cryostat commissioning was performed over the course of 5 major cooldown runs, which required

TABLE IV. Summary of the CUORE cryostat commissioning runs at LNGS. For each test run, goals and schedule are reported.

Run	Duration	Goals
	Oct 2012 - Jan 2014	- DU standalone tests
0	Jul 2012 - Aug 2013	- reach stable PT temperature
1	Sep 2013 - Oct 2014	- merge 4 K cryostat and DU - installation of inner plates and vessels - reach stable base temperature
2	Oct 2014 - Jan 2015	- installation of detector read-out wiring
3	Jan 2015 - Sep 2015	- Top Lead installation - TSP installation - cooldown with FCS
4	Jul 2015 - Mar 2016	- ILS installation - Mini-Tower performance optimization

about four years to complete (see Ref. [38] for details). The commissioning ended with the successful installation and cooldown of the CUORE detector.

A. Run 0

The construction of the 4 K outer cryostat, i.e. the 300 K, 40 K and 4 K stages [19], proceeded roughly in parallel with the separate commissioning of the DU. The goal of the first cooldown run, Run 0, was to verify the outer cryostat, both in terms of vacuum tightness and cooling power of the PT system.

The temperatures of the 40 K and 4 K plates from Run 0 are plotted in Fig. 12. As it can be seen from the figure, the initial temperature drop is much steeper for the 40 K plate. This is due to the smaller mass at the 40 K stage and to the higher cooling power of the PT first stage with respect to the second stage. Then, the slope flattens some tens of kelvin below ~ 100 K. The cooling of the 4 K proceeds more slowly and speeds up in the final part, after matching the 40 K stage temperature.

During the cooldown, significant thermal gradients can form across the vessels. Temperature differences of up to ~ 40 K were measured between the bottom and top of the 40 K vessel. However, by the end of the cooldown, the temperature gradients were measured to be $\lesssim 0.2$ K, which was in line with expectations from simulations.

In Run 0, stable temperatures of 32 K and 3.4 K were reached on the 40 K and 4 K stages after about 12 days.

TABLE V. CUORE cryostat part installation during the commissioning runs. The symbols \checkmark/\times indicate presence/absence of the various elements.

Part	Run 0	Run 1	Run 2	Run 3	Run 4
<i>Load structure</i>					
300 K, 40 K, 4 K	\checkmark	\checkmark	\checkmark	\checkmark	\checkmark
Still, HEX, MC	\times	\checkmark	\checkmark	\checkmark	\checkmark
TSP	\times	\times	\times	\checkmark	\checkmark
<i>Lead shields</i>					
Top Lead	\times	\times	\times	\checkmark	\checkmark
ILS	\times	\times	\times	\times	\checkmark
<i>Cooldown</i>					
DU	\times	\checkmark	\checkmark	\checkmark	\checkmark
PTs	3	4	4	5	5
FCS	\times	\times	\times	\checkmark	\checkmark
<i>Read out</i>					
WT ports	\checkmark	\checkmark	\checkmark	\checkmark	\checkmark
detector wiring	\times	\times	\checkmark	\checkmark	\checkmark
Mini-Tower	\times	\times	\checkmark	\checkmark	\checkmark

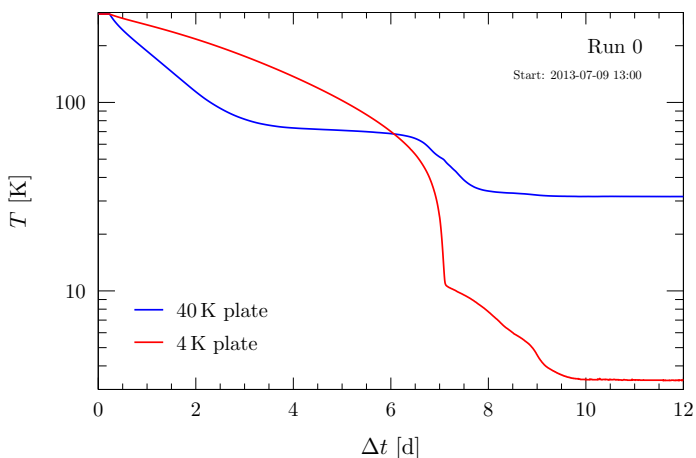


FIG. 12. Temperatures of the 40 K and 4 K stages during the cooldown of the 4 K outer cryostat in Run 0. The final temperatures of 32 K and 3.4 K are reached after 12 days. Below ~ 10 K (after day 7) the cooling rate is driven by a stainless steel mass that was being used to perform tests on the DCS. The much higher heat capacity of the stainless steel slows the cooldown relative to what it would have been in the absence of this test.

Based on these temperatures and cooling time, Run 0 was considered a successful test of the 4 K outer cryostat.

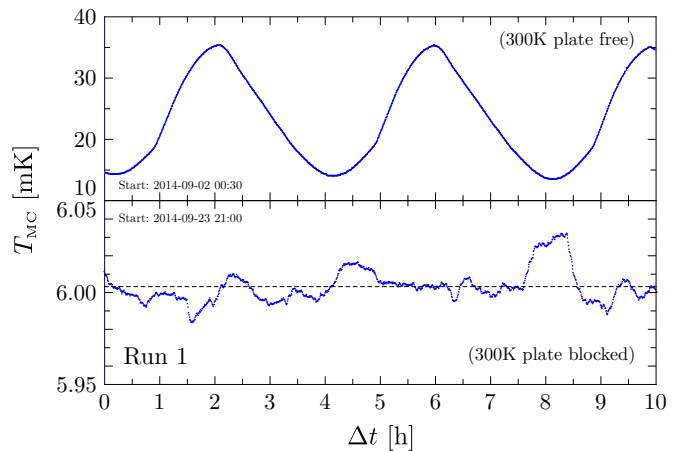


FIG. 13. Temperature of the MC plate during Run 1. (Top) The 300 K plate has no constraints in the horizontal plane. the temperature oscillates over more than 20 mK with a period of ~ 4 h and does not reach 10 mK. (Bottom) The 300 K plate is anchored to the MSP. The MC reaches a stable base temperature of (6.00 ± 0.01) mK.

B. Run 1

The Still, HEX and MC plates and vessels were installed in the next phase of commissioning, along with the integration of the DU. The Run 1 cooldown was a test of the performance of the “complete” cryostat.

After ~ 11 days of cooldown, the 40 K and 4 K stages reached stable temperatures of 34.9 K and 3.8 K, at which point the DU took over and completed the cooldown to base temperature in less than one day. However, we initially observed large oscillations in the base temperature, reaching up to ~ 35 mK with a ~ 4 h period. This can be seen in the upper panel of Fig. 13.

We determined that this instability was due to mechanical vibrations from the PTs causing micro-friction and dissipating heat on the Still, HEX and MC stages. This was tested through a series of diagnostic measurements with vibrational sensors installed on the 300 K plate.

To mitigate this effect, we installed a bracket system which rigidly anchored the 300 K plate (see Sec. V F). Three iron brackets were directly mounted to the 300 K plate; each one pushing against another bracket, which was mounted to the MSP. This approach dramatically suppressed the temperature oscillations, as can be seen the bottom of Fig. 13. With these anchors installed, we were able to reach a satisfactory stable base temperature of 6 mK, with the Still and HEX at 1 K and 35 mK, respectively.

C. Run 2

The next step of the commissioning consisted of the installation of the CUORE detector readout wiring, with the related boxes for the connection between the bolome-

ters and the front end electronics. This was tested in Run 2.

The detector wiring consists of woven ribbon cables with twisted pairs of NbTi wires in a NOMEX™ texture, for a total of ~ 2600 wires [8, 9]. The wiring creates a link between the coldest stage and the external environment. Although the wiring had already been tested in dedicated setups, it was fundamental to verify the actual impact on the cryogenic performance of the CUORE cryostat.

The wire thermalization down to 4 K occurs via radiation transmission along the PTFE spirals inside the WT ports. Below, ribbons from the same WT are sandwiched between gold-plated copper clamps installed above and below the Still and HEX plates. On the MC, the junction boxes for the connection between the ribbons and the cabling from the bolometers act as thermalizers. Measurements of the temperatures, both on the plates and along the wires, showed values in line with the expectations and the cooldown was considered successful.

Run 2 also provided the first possibility to run a bolometric detector inside the CUORE cryostat. The Mini-Tower was the equivalent of a 2-floor CUORE tower and was mounted directly to the MC plate (rather than the TSP, which was not yet installed). Since the MC is coupled directly to the cryostat structure and is thus relatively noisy in terms of vibrations, we did not expect to be able to observe physical events on the Mini-Tower. However, this was an opportunity to observe the behavior and performance of NTD sensors.

During the cooldown of Run 2, a superleak was discovered in the DU circuit.⁷ This required extracting the DU from the CUORE cryostat and moving it back to its test cryostat, which can be thermally cycled much faster and allows for a much faster diagnosis. After identifying the source of the leak, the DU was repaired and reinstalled into the CUORE cryostat and we could move to the next step in the commissioning.

D. Run 3

Run 3 tested the installation of the TSP and the Top Lead, which was assembled in an external cleanroom facility, and provided the first opportunity to employ the FCS. The run proved successful. The cooldown time was consistent with previous runs and the addition of the new stages did not negatively impact the cryogenic performance. The thermometry confirmed that the TSP and the Top Lead were consistent with the stages to which they were thermalized. The temperature of the Top Lead and HEX stage (to which the Top Lead is thermalized) is plotted in Fig. 14.

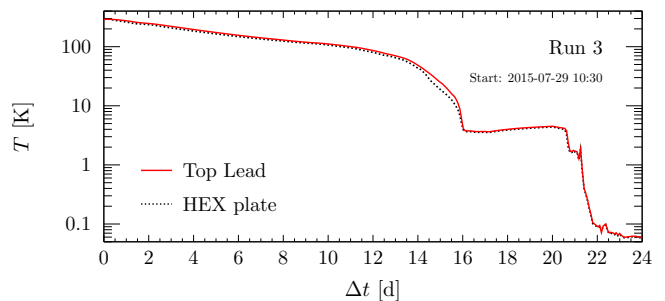


FIG. 14. Temperature of the Top Lead during the cooldown of Run 3. The HEX plate temperature is shown as a reference. The effect of turning off the FCS on day 14 is clearly visible as a slightly worsening of the lead thermalization process. This immediately recovers once the lead becomes superconductive at $T_c(\text{Pb}) = 7.2$ K.

E. Run 4

The preparation for Run 4 began with the assembly of the ILS [24]. After completion of Run 3 and the opening of the cryostat, the ILS was installed. This operation took place inside a dedicated cleanroom environment which had been assembled under the CUORE cryostat.

The cooldown of Run 4 was successful. The performance of the FCS can be seen in Fig. 15. The cooldown started with a higher compressor frequency, and therefore a larger gas flow. The motor speed had to be reduced when the difference between the He temperatures at the IVC input and exit became too small. In fact, since the system was getting colder, the GM coolers were unable to keep up with the enthalpy being extracted from the cryostat. In the end, the large thermal load of the cryostat, as well as thermal loads on the FCS lines themselves, forced us to switch the FCS off when the temperature of the 4 K stage dropped below the input He temperature. The PTs were started on day 3 of the cooldown, which translated into a dramatic improvement in the cooldown speed on the cryostat. We estimated that within one day, the PTs were already providing $\sim 1/3$ of the cooling power.

Within about 22 days, the 40 K and 4 K stages reached stable temperatures of 34.5 K and 3.4 K respectively. The final temperature of the ILS was compatible with that measured on the 4 K stage (Fig. 16).⁸

During Run 4, we performed a characterization of the DU with the “fully loaded” cryostat (with the exception of the detector). The new measured cooling power was close to that originally measured (Fig. 11), despite the additional thermal loads. Its value was $3 \mu\text{W}$ at 10 mK, obtained with an optimal mixture flow within the range $(1010 - 1020) \mu\text{mol s}^{-1}$. The long duration of Run 4 also

⁷ A superleak is a leak that is permeable to superfluid ^4He due to its superfluidity, but not to ^3He .

⁸ As can be seen in Fig. 16, we reached these temperatures within ~ 17 days, however, due to some problems related to the compressor cooling water, it actually took a few more days to stabilize the temperature.

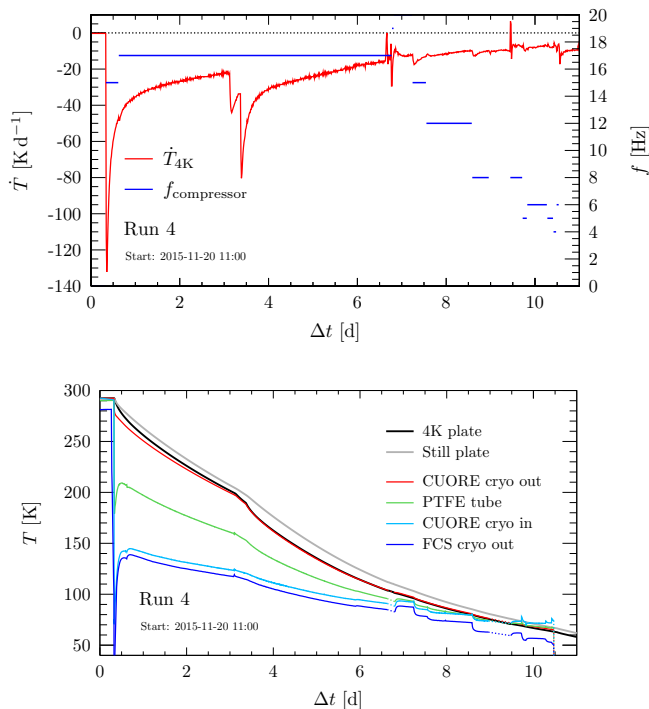


FIG. 15. (Top) Detail of the cooling rate with the FCS during Run 4. The compressor starts at a higher motor frequency, and this is periodically reduced over the course of the FCS operation. The improvement in the cooling obtained with the frequency tuning are visible on days 7, 8 and 9. The PTs are turned on on day 3. The irregular behavior on days 6 and 9 is due to instabilities of the compressor cooling. (Bottom) Time profile of the FCS temperatures in key points of the circuit. The 4 K and Still temperatures are plotted as references. The FCS cooling is effective until the temperature of the gas entering the CUORE cryostat is no longer colder than the 4 K/Still plates on day 9. The difference between the temperatures measured at the exit of the FCS cryostat and at the entrance of the CUORE cryostat is caused by parasitic thermal loads on the FCS lines themselves.

allowed us to test the stability of the MC base temperature on the timescale of a few months, which maintained an average value of 6.3 mK.

In Run 4, the Mini-Tower was mounted to the TSP, identically to the way the eventual CUORE detector would be. A large part of this run was devoted to the understanding of the noise generation and propagation through real-time analysis of the noise on the Mini-Tower bolometers. By monitoring the variation in intensity and frequency of noise peaks in the bolometer noise power spectra, it was possible to identify sources of vibrational and mechanical noise and find solutions to mitigate them. Many of these solutions pushed in the direction of increasing the rigidity of the cryostat structure.

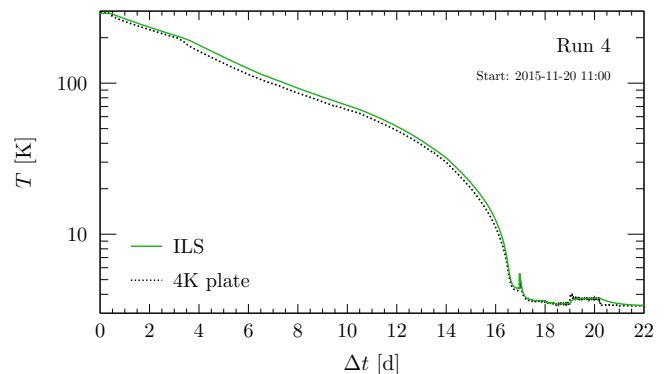


FIG. 16. Temperature of the ILS during the Run 4 cooldown. The 4 K plate temperature is shown as a reference. The effect of turning on the PTs on day 3 is clearly visible as a faster cooling of the latter stage.

F. New implementations after the commissioning

As discussed in Sec. II, the design of the CUORE cryostat had to satisfy a series of demanding and sometimes countervailing requirements. The outcome was a cryogenic infrastructure that is unique in its kind. In this sense, the CUORE cryostat is a prototype. From a practical point of view, this means that it was not always possible to accurately foresee every challenge at the design stage. To this extent, the commissioning phase proved invaluable in terms of gaining the experience to diagnose, correct and operate the CUORE cryostat. It also allowed us to modify some choices made in the initial design.

The major adjustment with respect to the initial cryostat design concerned the rigidity of the support structure. The suspension system was designed to isolate the cryostat infrastructure from mechanical vibrations, however, during the commissioning runs, this proved to present a problem for maintaining a stable base temperature. We determined that the entire cryostat was behaving like an articulated pendulum, and the friction generated by the relative movement of plates was creating a large heat load, leading to an unstable base temperature. These oscillations were being driven by the PTs, despite the attempts to suspend the PT motor heads and dissipate these forces elsewhere.

Among the modifications to counter these oscillations, we decided to prevent relative motion of the plates by fixing parts of the joints, and to reduce the motion of the 300 K plate by fixing it to the MSP (Sec. VB). These solutions provided a more efficient path to dissipate the energy imparted by the PTs rather than allowing it to grow into a sizable oscillation. This was necessary to operate a bolometric detector, as became evident during the operation of the Mini-Tower.

We also observed that the seismic dampers supporting the entire cryostat infrastructure (see Fig. 2), had resonant oscillation frequencies in the (1–3) Hz range, which lies right in the middle of the CUORE signal bandwidth.

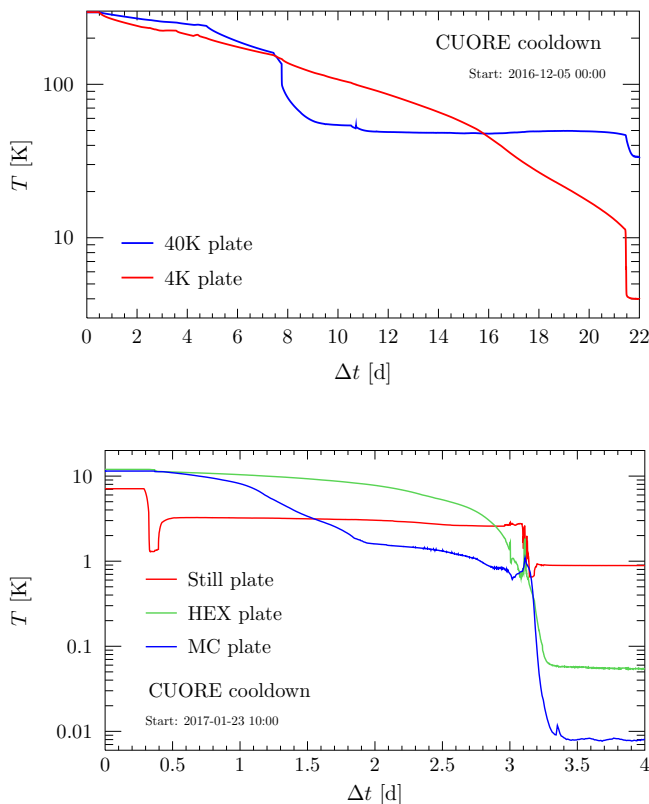


FIG. 17. CUORE cooldown. (Top) Temperatures of the 40 K and 4 K stages as a function of time since the turn on of the FCS. The stages reach temperatures of 33.6 K and 4.0 K after ~ 22 d. The sudden changes in cooling rates of both stages seen around day 4 is due to the starting of the PTs. The FCS was turned off on day 10. (Bottom) IVC stage temperatures as a function of time since the start of the DU circulation. The base temperature achieved on the MC with the full experiment apparatus is 8 mK, with 0.89 K and 55 mK on the Still and HEX stages, respectively. The initial Still temperature drop and rise within the first day is due to the switch from ^4He to ^3He circulation. By day 3, the gas has fully condensed and the dilution cooling takes over. This is visible as the small spike in the MC temperature.

To mitigate this, we designed and installed a “mechanical fuse” system, which prevents the growth of small oscillations, but will break away in the case of a strong acceleration (such as an earthquake). This consists of a series of thin steel plates inserted between the concrete support structure and the foundation. This system allows us to reduce mechanical vibrations, while still satisfying the seismic safety of the structure.

After these changes, we could finally proceed towards the installation of the CUORE detector.

VI. CUORE COOLDOWN

After the installation of the CUORE detector, the closing of the cryostat was made significantly more compli-

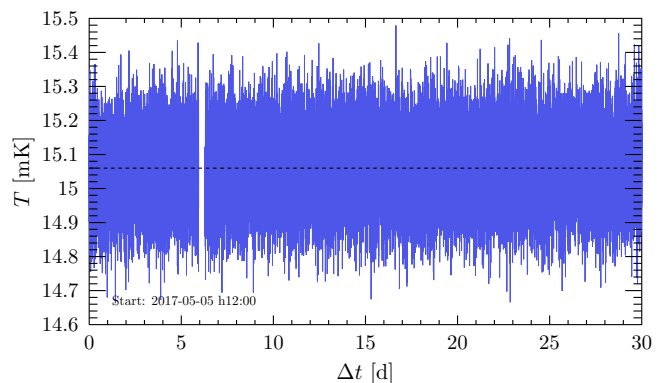


FIG. 18. Base temperature stability over a thirty day period while the cryostat was “undisturbed” during the initial phase of the CUORE data taking. The MC temperature is (15.06 ± 0.10) mK. The dashed line indicates the average value. The gap on day 6 is due to hardware operation the cryogenic system.

cated. The mounting of the towers to the TSP took place inside a dedicated cleanroom environment, which was flushed with Rn-free air [39]. This cleanroom was kept in place while closing the inner cryostat vessels up to the 4 K shield. Once the 4 K vessel was closed, the IVC could be pumped and the detector could be protected from contact with Rn by the vacuum. Once closed, both the 4 K and 40 K vessels and plates had to be covered with new layers of superinsulation. The old superinsulation that had been in use for the cryostat commissioning, and was now dirtier after years of exposure to air and continuous handling, had been removed to allow the cleaning of the vessels.

The progression of the CUORE cooldown is shown in Fig. 17. As usually, this began with the FCS, while the PTs were turned on after a few days. The FCS was then turned off and disconnected once the thermal stages reached ~ 150 K. As expected, the cooldown took ~ 20 days before turning on the DU unit. We paused the cooldown for about one month to perform some debugging of the detector electronics and to address a leak that had formed in the dilution circuit (outside the cryostat). Once the DU was turned on, it took less than 4 days to reach the base temperature of 8 mK on the MC, with 0.89 K and 55 mK on the Still and HEX stages respectively.

An initial scan of the detector behavior at various temperatures identified 15 mK as a suitable operating temperature. Fig. 18 shows the stability of the system for over one month of operation. The CUORE cooldown and the beginning of the detector operation successfully concluded the commissioning of the CUORE cryostat.

The analysis of the first collected physics data provided a measurement of the background in the $0\nu\beta\beta$ decay region [2]. The observed value, (0.014 ± 0.002) counts $\text{keV}^{-1} \text{kg}^{-1} \text{yr}^{-1}$, was in line with the expectations derived from the background model [10]. The

strict material selection and the dedicated construction techniques for the cryostat components resulted in a cryogenic system fully compliant with the design goals.

VII. SUMMARY

The CUORE cryostat was designed to satisfy a wide set of very stringent requirements, ranging from cryogenic performance and duty cycle, to vibration isolation and mechanical stability, and to low radioactive content and shielding. The full construction and assembly of the cryostat itself took more than three years. The commissioning phase was long and complex, requiring several cooldowns to integrate the numerous custom components.

On the cryogenics side, the success of the CUORE cryostat was demonstrated by the cooldown of the CUORE detector to 8 mK, and by the ability to operate stably at 15 mK. At the same time, the measured background in the $0\nu\beta\beta$ decay region, (0.014 ± 0.002) counts $\text{keV}^{-1} \text{kg}^{-1} \text{yr}^{-1}$, is in line with the CUORE sensitivity goal and does not show any excess due to the cryogenic system. This proves the effectiveness of the material selection and construction techniques for the cryostat components.

The CUORE cryostat has set the stage for one of the most sensitive searches for $0\nu\beta\beta$ decay. More generally, it demonstrated the ability to cool tonne-scale detectors to temperatures of a few mK, and operate them in low-noise and low-background environments compatible with the requirements for rare-event searches. This marks a major milestone in the history of low-temperature detector techniques.

ACKNOWLEDGMENTS

We wish to express our gratitude to the entire CUORE Collaboration for the invaluable support. Thanks are due to the Laboratori Nazionali del Gran Sasso for generous hospitality. We thank Leiden Cryogenics for designing and constructing our high-performance Dilution Unit and the Fast Cooling System, and the patient and continuous support during the cryogenic system commissioning. We gladly acknowledge the help of S. Parmeggiano, P. Mereu and G. Giraudo in various stages of the construction. We thank Low T-Solutions and TCSservice s.p.a. for the ingenuous and continuous support in the commissioning phase. We would like to thank A. Benoit,

M. Bühler, P. Camus, E. Coccia, C. Gargiulo, P. van der Linden, N. Mirabolfathi, P. Negri, P. Rapagnani and A. Woodcraft for the reviews and invaluable feedback on the design and implementation of the cryogenic systems, and the members of the LNGS Scientific Committee and of the international CUORE Review Committee for the continuous oversight and support during the design, construction, and operations of the CUORE experiment. This work was supported by the Istituto Nazionale di Fisica Nucleare (INFN); the National Science Foundation under Grant Nos. NSF-PHY-0605119, NSF-PHY-0500337, NSF-PHY-0855314, NSF-PHY-0902171, NSF-PHY-0969852, NSF-PHY-1307204, NSF-PHY-1314881, NSF-PHY-1401832, and NSF-PHY-1404205; the Alfred P. Sloan Foundation; the University of Wisconsin Foundation; and Yale University. This material is also based upon work supported by the US Department of Energy (DOE) Office of Science under Contract Nos. DE-AC02-05CH11231, DE-AC52-07NA27344, and DE-SC0012654; and by the DOE Office of Science, Office of Nuclear Physics under Contract Nos. DE-FG02-08ER41551 and DE-FG03-00ER41138. This research used resources of the National Energy Research Scientific Computing Center (NERSC).

APPENDIX: Glossary

Here, we list the acronyms related to the CUORE cryogenic system and its components that have been introduced and used throughout this work:

DCS	Detector Calibration System
DU	Dilution Unit
DS	Detector Suspension
GM	Gifford-McMahon (cryocooler)
HEX	Heat EXchanger
ILS	Inner Lead Shield
IVC	Inner Vacuum Chamber
FCS	Fast Cooling System
LS	Lead Suspension
MC	Mixing Chamber
MSP	Main Support Platform
NTD	Neutron Transmutation Doped
OVC	Outer Vacuum Chamber
PT	Pulse Tube
TSP	Tower Support Plate
WT	Wire Tray

[1] K. Alfonso *et al.* (CUORE Collaboration), *Phys. Rev. Lett.* **115**, 102502 (2015).
 [2] C. Alduino *et al.* (CUORE Collaboration), *Phys. Rev. Lett.* **120**, 132501 (2018).

[3] C. Alduino *et al.* (CUORE Collaboration), *J. Instrum.* **11**, P07009 (2016).
 [4] C. Alduino *et al.* (CUORE Collaboration), *Eur. Phys. J. C* **77**, 532 (2017).

- [5] J. S. Cushman *et al.*, *Nucl. Instrum. Meth. A* **844**, 32 (2017).
- [6] E. Andreotti *et al.*, *Astropart. Phys.* **34**, 822 (2011).
- [7] C. Arnaboldi *et al.* (Cuoricino Collaboration), *Phys. Rev. C* **78**, 035502 (2008).
- [8] E. Andreotti *et al.*, *J. Instrum.* **4**, P09003 (2009).
- [9] A. Giachero, C. Gotti, M. Maino, and G. Pessina, *Nucl. Instrum. Meth. A* **718**, 229 (2013).
- [10] C. Alduino *et al.* (CUORE Collaboration), *Eur. Phys. J. C* **77**, 543 (2017).
- [11] R. Ardito and F. Perotti, “Seismic analysis of support structure for the CUORE experiment cryostat (in Italian),” (2011 and 2018), Report of the Polytechnic University of Milan.
- [12] C. Bucci, P. Carniti, L. Cassina, C. Gotti, A. Pelosi, G. Pessina, M. Turqueti, and S. Zimmermann, *J. Instrum.* **12**, P12013 (2017).
- [13] M. Barucci, L. Lolli, L. Risegari, and G. Ventura, *Cryogenics* **48**, 166 (2008).
- [14] M. Vanzini *et al.*, *Nucl. Instrum. Meth. A* **461**, 293 (2001).
- [15] A. D’Addabbo, C. Bucci, L. Canonica, S. Di Domizio, P. Gorla, L. Marini, A. Nucciotti, I. Nutini, C. Rusconi, and B. Welliver, *Cryogenics* **93**, 56 (2018).
- [16] <https://www.minusk.com>.
- [17] A. Bersani *et al.*, “The CUORE Detector Suspension,” (2019) [paper in preparation].
- [18] A. Bersani, L. Canonica, M. Cariello, R. Cereseto, S. Di Domizio, and M. Pallavicini, *Cryogenics* **54**, 50 (2013).
- [19] F. Alessandria *et al.*, *Nucl. Instrum. Meth. A* **727**, 65 (2013).
- [20] <https://www.aurubis.com/products/page-shapes>.
- [21] M. Schwark, F. Pobell, W. P. Halperin, C. Buchal, J. Hanssen, M. Kubota, and R. M. Mueller, *J. Low Temp. Phys.* **53**, 685 (1983).
- [22] M. Koláč, B. S. Neganov, and S. Sahling, *J. Low Temp. Phys.* **59**, 547 (1985).
- [23] M. Martinez *et al.*, *AIP Conf. Proc.* **1185**, 693 (2009).
- [24] C. Bucci *et al.*, “The Roman lead shield of the CUORE experiment,” (2019) [paper in preparation].
- [25] A. Alessandrello *et al.*, *Nucl. Instrum. Meth. B* **142**, 163 (1998).
- [26] American Society of Mechanical Engineers (ASME), *Boiler & Pressure Vessel Code* (2010), Sec. VIII, Div. 1.
- [27] <https://www.ansys.com>.
- [28] <https://technetics.com/products/sealing-solutions/metal-seals/helicoflex>.
- [29] J. W. Arblaster, *J. Phase Equil. Diff.* **36**, 422 (2015).
- [30] J. W. Arblaster, *Comput. Coupling Phase Diagrams Thermochem.* **39**, 47 (2012).
- [31] G. K. White, S. Collocott, and J. G. Collins, *J. Phys. Condensed Matter* **2**, 7715 (1990).
- [32] C. Pagliarone, L. Cappelli, C. Bucci, P. Gorla, D. D’Aguanno, F. Marignetti, G. Erme, and S. Kartal, *PoS EPS-HEP2017*, 634 (2018).
- [33] C. Bucci *et al.*, “CUORE Fast Cooling,” (2019) [paper in preparation].
- [34] <http://www.cryomech.com/cryorefrigerators/gifford/al600>.
- [35] <http://www.cryomech.com/cryorefrigerators/pulse-tube/pt415/>.
- [36] <https://leiden-cryogenics.com/products/cryogen-free>.
- [37] <http://www.magnicon.com/squid-systems/noise-thermometer>.
- [38] S. Dell’Oro, *Ph.D. thesis, INFN - Gran Sasso Science Institute* (2019).
- [39] G. Benato *et al.*, *J. Instrum.* **13**, P01010 (2018).